JGR Space Physics

RESEARCH ARTICLE
10.1029/2023JA031303

Interplanetary Magnetic Field B_y Controls the Magnetopause Location

M. Aghabozorgi Nafchi[1], F. Němec[1], G. Pi[1], Z. Němeček[1], J. Šafránková[1], K. Grygorov[1], and J. Šimůnek[2]

[1]Faculty of Mathematics and Physics, Charles University, Prague, Czech Republic, [2]Institute of Atmospheric Physics of the Czech Academy of Sciences, Prague, Czech Republic

Key Points:

- Nearly 15,000 magnetopause crossings are used to study the influence of interplanetary magnetic field (IMF) on the magnetopause location
- The orientation of IMF B_y component becomes significant at the times of low Alfvén Mach number, introducing a dawn-dusk asymmetry
- Magnetopause distances are larger in the IMF direction, consistently with available magnetohydrodynamic simulations

Supporting Information:

Supporting Information may be found in the online version of this article.

Correspondence to:

M. Aghabozorgi Nafchi, maryam.aghabozorgi-nafchi@matfyz.cuni.cz

Citation:

Aghabozorgi Nafchi, M., Němec, F., Pi, G., Němeček, Z., Šafránková, J., Grygorov, K., & Šimůnek, J. (2023). Interplanetary magnetic field B_y controls the magnetopause location. *Journal of Geophysical Research: Space Physics*, *128*, e2023JA031303. https://doi.org/10.1029/2023JA031303

Received 9 JAN 2023
Accepted 22 APR 2023

Author Contributions:

Data curation: K. Grygorov, J. Šimůnek
Formal analysis: M. Aghabozorgi Nafchi
Investigation: M. Aghabozorgi Nafchi, F. Němec, G. Pi, Z. Němeček, J. Šafránková
Methodology: F. Němec
Project Administration: Z. Němeček, J. Šafránková
Software: M. Aghabozorgi Nafchi
Supervision: F. Němec, G. Pi
Validation: F. Němec, G. Pi
Visualization: M. Aghabozorgi Nafchi

Abstract We present a statistical study of interplanetary magnetic field (IMF) effects on the magnetopause location based on nearly 15,000 magnetopause crossings identified in the THEMIS A-E, Magion 4, Geotail, and Interball-1 satellite data. In order to exclude the dominant controlling role of the solar wind dynamic pressure, differences between observed and empirical model magnetopause distances are analyzed. We find that the magnetopause distance is significantly controlled by the IMF clock angle, not considered in the used empirical models. Furthermore, during very low Alfvén Mach numbers ($M_A < 4$), IMF B_y component can induce a considerable dawn-dusk asymmetry of the magnetopause shape. The magnetopause distance is found to be larger in the direction of the IMF vector, that is, not only the magnitude but also the orientation of the IMF B_y component is eventually important. The obtained results are qualitatively consistent with a magnetohydrodynamic model run at the Community Coordinated Modeling Center.

1. Introduction

The magnetopause is the boundary between the magnetosphere and the shocked solar wind in the magnetosheath. It corresponds to the farthest location reached by terrestrial magnetic field and processes at the magnetopause control ultimately the solar wind energy coupling to the magnetosphere (e.g., Haaland et al., 2021). Neither the location nor the shape of the magnetopause is constant in time, being dependent on many different factors. These include the upstream solar wind parameters as well as the internal state of the magnetosphere (e.g., Němeček et al., 2020).

The first observations of the magnetopause date back to the very beginning of the space era. Early mapping of the boundary position was possible using data obtained by the three-component magnetometer carried on board the Explorer 12 spacecraft (Cahill & Amazeen, 1963). At the same time, basic magnetohydrodynamic (MHD) understanding of the solar wind interaction with the geomagnetic field was formed (Spreiter et al., 1966). Several hundreds of magnetopause crossings obtained by the Interplanetary Monitoring Platform spacecraft eventually allowed the construction of the first empirical models of the magnetopause location (Fairfield, 1971).

The idea of empirical magnetopause models based on identified boundary crossings was further applied by Formisano et al. (1979), who used nearly 1,000 magnetopause crossings identified by several different spacecraft and rather general second order surface to obtain the magnetopause model parameterized by the solar wind dynamic pressure. Subsequent popular magnetopause models developed by Petrinec and Russell (1996) and Shue et al. (1997) assumed a cylindrical symmetry around the direction of the incoming solar wind and, on top of the solar wind dynamic pressure, considered also the magnetopause location dependence on the interplanetary magnetic field (IMF) B_z component. At locations out of the ecliptic plane, magnetopause cusp indentations eventually introduce a considerable asymmetry (Šafránková et al., 2002) and the dipole tilt angle becomes important (Boardsen et al., 2000; Šafránková et al., 2005). Some of the more recent empirical models thus use more complicated mathematical forms to attempt to describe the three-dimensional asymmetric magnetopause shape (Lin et al., 2010).

Apart from the solar wind dynamic pressure and IMF B_z component, the direction of the IMF appears to be an important parameter controlling the magnetopause location. Dušík et al. (2010) demonstrated a systematic increase of the magnetopause distance for the radial IMF direction. This was subsequently explained by considering the IMF effect on the magnetosheath, which is the region ultimately exerting the pressure on the subsolar magnetopause (Samsonov et al., 2012). Case and Wild (2013) used nearly 3,000 of magnetopause crossings

Writing – original draft: M. Aghabozorgi Nafchi
Writing – review & editing: F. Němec, G. Pi, Z. Němeček, J. Šafránková

identified in the Cluster spacecraft data to investigate the performance of various models and importance of several selected parameters. They concluded that the IMF clock angle has little to no influence on the radial difference between the observed and model boundary crossings, essentially meaning that the model parameterization by IMF B_z appeared sufficient. On the other hand, a recent massive multi-mission statistical study revealed the importance of IMF B_y component for the magnetopause surface flaring (Nguyen et al., 2021a, 2021b).

Global MHD simulations were used to investigate the effect of IMF by Lu et al. (2013) and Liu et al. (2015). They revealed that, apart from the flaring angle, the IMF controls also the magnetopause azimuthal asymmetry. They found that the magnetopause cross-section tends to be elongated along (or opposite) to the IMF direction, while it tends to be shrunk in the direction perpendicular to the IMF direction. Lavraud and Borovsky (2008) investigated the solar wind-magnetosphere interaction, including the magnetosheath conditions, and argued that the magnetopause asymmetry would be particularly pronounced at the times of low Alfvén Mach numbers (M_A). Their subsequent analysis of magnetopause crossings seems to indeed confirm this prediction. While the magnetopause appears to be generally circular during high M_A, it becomes elongated (albeit with only moderate statistical significance) along the IMF direction during low M_A (Lavraud et al., 2013). The origin of this asymmetry is possibly related to the asymmetries in the magnetosheath region (Longmore et al., 2005; Turc et al., 2020) exerting the pressure upon the magnetosphere. Alternatively, one may also consider possible asymmetry related to the magnetosphere, for example, asymmetrical terrestrial ring current (Dmitriev et al., 2004). Ionospheric conductivity (Němeček et al., 2016), as well as thermal (Grygorov et al., 2022), and energetic (Machková et al., 2019) magnetospheric plasma are among the magnetospheric phenomena known to affect the magnetopause location, in particular during geomagnetically disturbed periods.

In this study, we use a database of nearly 15,000 magnetopause crossings identified in data obtained by several different spacecraft to investigate the effect of the IMF B_y component on the location of the magnetopause. We demonstrate that, at the times of low M_A, a significant dawn-dusk asymmetry is induced. The magnetopause appears not to be symmetrically elongated, but rather extending to larger distances in one direction, depending on the IMF orientation. We further compare the experimental results with a MHD model run at the Community Coordinated Modeling Center (CCMC), obtaining qualitative agreement. The used data set of magnetopause crossings is described in Section 2. The obtained results are presented in Section 3 and they are discussed in Section 4. Finally, Section 5 contains the summary.

2. Data

The presented analysis is based on as many as 49,638 magnetopause crossings identified in the THEMIS A-E, Magion 4, Geotail, and Interball-1 satellite data obtained between 1995 and 2020. The magnetopause crossings in the THEMIS data were identified using an automated routine that searched for simultaneous changes of magnetic field and plasma parameters (Grygorov et al., 2022; Němeček et al., 2016). All the identified candidate crossings were eventually verified by a visual inspection of the plots, and possible false positives were removed from the data set. The list of magnetopause crossings in the older spacecraft data was compiled manually (Šafránková et al., 2002).

Projections of individual magnetopause crossings to the Geocentric Solar Magnetospheric x-y plane are shown in Figure 1a. The subsolar region, corresponding to solar zenith angles (i.e., the angles between positional vectors and x-axis) lower than 30°, is marked by the solid lines. Only the data measured within this region are considered hereinafter, corresponding to as many as 14,781 crossings. The reason is that, due to the limited apogee distance of the THEMIS spacecraft and related insufficient sampling of large distances, the magnetopause crossings identified at larger solar zenith angles become biased toward lower distances. A distribution of considered magnetopause crossings as a function of the z_{GSM} coordinate is presented in Figure 1b. It can be seen that most of the crossings occur close to the ecliptic plane (where the effect of cusp indentations is negligible).

3. Results

For each of the crossings, its location (x_{GSM}, y_{GSM}, z_{GSM}) and selected solar wind parameters obtained from the Wind spacecraft were added to the database for the further analysis. The time lag due to the solar wind propagation from the Wind spacecraft to the subsolar magnetopause is considered by the two-step propagation method (Šafránková et al., 2002). The solar wind parameters include the three components of the IMF (B_x, B_y, B_z), the

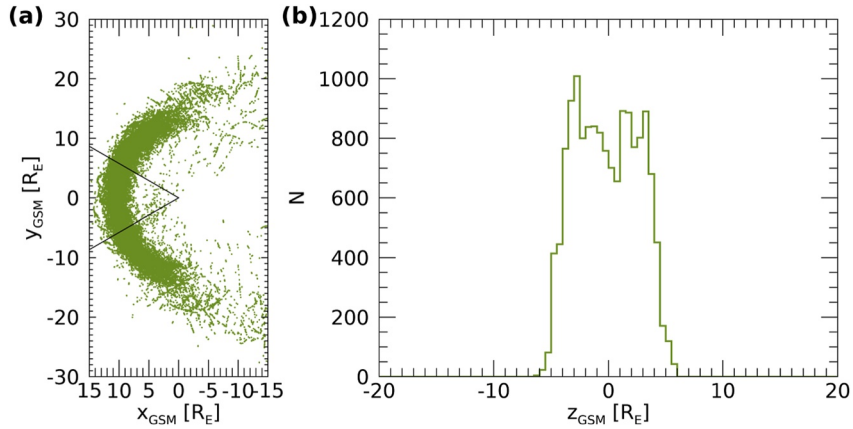

Figure 1. (a) Projections of individual identified magnetopause crossings to the Geocentric Solar Magnetospheric *x*-*y* plane. The subsolar region, corresponding to solar zenith angles lower than 30°, is marked by the solid lines. (b) Histogram of the z_{GSM} coordinate of magnetopause crossings identified in the subsolar region.

plasma density, velocity vector (v_x, v_y, v_z), and dynamic pressure. The dynamic pressure calculation assumes a constant 4% alpha particle content in the solar wind.

The most significant factor controlling the magnetopause location is clearly the solar wind dynamic pressure, followed by the IMF B_z component. In order to account for their effects and to allow the investigation of additional, less important factors, we analyze the differences between observed and model radial distances rather than the radial distances themselves. Provided that the used model does not consider the parameter we intend to study, this is an effective way of accounting for the dynamic pressure and IMF B_z dependences. Three different empirical models parameterized by the dynamic pressure and IMF B_z are considered, all ultimately providing qualitatively the same results. These models are: (a) Petrinec and Russell (1996), (b) Shue et al. (1997), and (c) Lin et al. (2010). Note that while the first two models assume the magnetopause to be cylindrically symmetric around the direction of the incoming solar wind, the third model considers a more complicated three-dimensional magnetopause shape accounting for the cusp indentations. Nevertheless, as the analyzed magnetopause crossings are limited to the subsolar region, the performance of all the three models when applied to our data set is found to be about the same.

Figure 2a shows the differences between observed and model magnetopause distances ($R_{Obs} - R_{Model}$) as a function of the IMF clock angle (= arctan(B_y/B_z)). Each point in the figure represents a single magnetopause crossing.

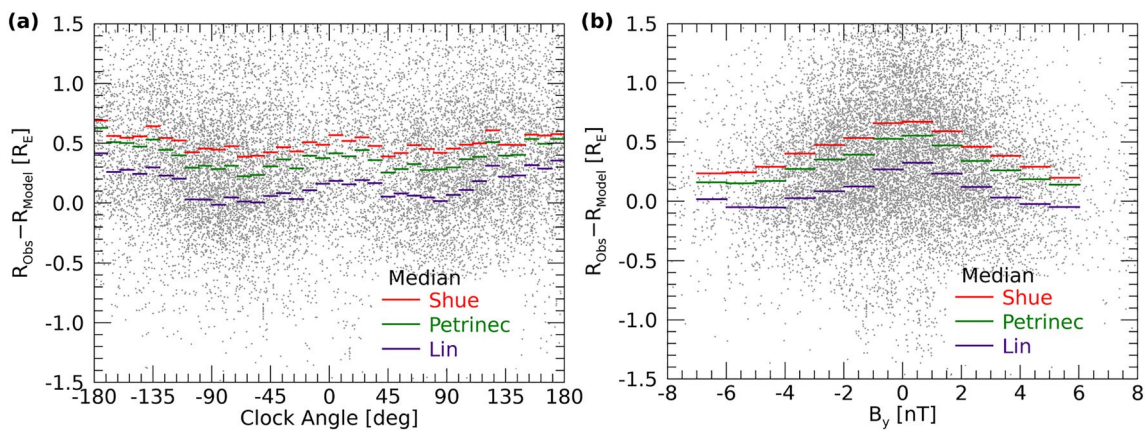

Figure 2. (a) Differences between observed and model magnetopause distances as a function of the interplanetary magnetic field (IMF) clock angle. Each point corresponds to a single magnetopause crossing, with the average value of the model magnetopause distance predicted by the three models used for the calculation of the ordinate. Median values of the differences between observed and model magnetopause distances obtained for individual models in respective abscissa intervals are shown by the horizontal lines. (b) The same as panel (a), but for the dependence on the IMF B_y.

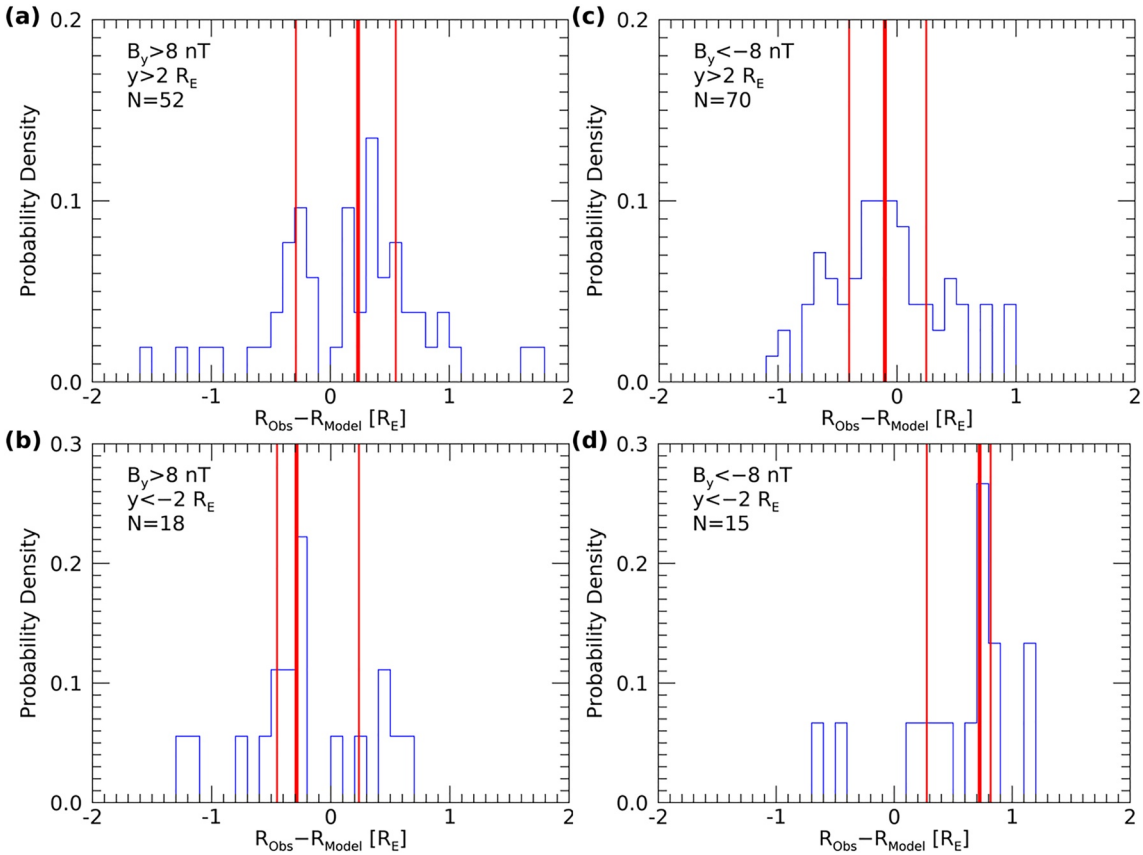

Figure 3. Histograms of differences between observed and model magnetopause distances for magnetopause crossings at (a) $B_y > 8$ nT and $y_{GSM} > 2\ R_E$, (b) $B_y > 8$ nT and $y_{GSM} < -2\ R_E$, (c) $B_y < -8$ nT and $y_{GSM} > 2\ R_E$, and (d) $B_y < -8$ nT and $y_{GSM} < -2\ R_E$. The thick and thin vertical red lines show the respective median values and 0.25/0.75 quartiles of the differences between observed and model magnetopause distances.

Since the prediction of the magnetopause distance depends on the model, we used predictions of the three above mentioned models and computed average value that serves as R_{Model} for individual crossings (the results obtained separately for each model are shown in Figure S1 in Supporting Information S1). Additionally, the median values of $R_{Obs} - R_{Model}$ in clock angle bins obtained for the individual magnetopause models are shown by the color segmented lines. It can be seen that while the clock angle dependences of $R_{Obs} - R_{Model}$ obtained for all the three models are qualitatively the same, they differ in the absolute values of the median $R_{Obs} - R_{Model}$. This difference is caused by functional forms of the magnetopause shape used in the models and thus it is not important in our study that investigates the effect of the IMF clock angle. However, it can be seen that the observed magnetopause distances tend to be larger when the IMF clock angle is close to 0 and $\pm 180°$ (i.e., northward or southward). On the other hand, the observed magnetopause distances tend to be smaller when the IMF clock angle is around $\pm 90°$ (i.e., eastward or westward). Considering qualitatively the same dependence obtained for all the three models, and taking into account that none of these models includes the clock angle as a parameter, this demonstrates that the IMF clock angle eventually affects the magnetopause distance. The importance of the IMF orientation is further confirmed in Figure 2b, which uses the same format to analyze the dependence of $R_{Obs} - R_{Model}$ on the IMF B_y component. R_{Obs} tends to be larger than R_{Model} for small IMF B_y, which is consistent with the results obtained in Figure 2a.

We further investigate the magnetopause location differences from the model predictions during extreme values of the IMF B_y component. Only the crossings under IMF $B_y < -8$ nT (136 crossings) and under IMF $B_y > 8$ nT (121 crossings) are considered. The obtained results are shown in Figure 3. It depicts histograms of $R_{Obs} - R_{Model}$ at given locations under given IMF B_y values. The values of R_{Model} are calculated as the average of the three aforementioned empirical model predictions. We note that qualitatively the same results are obtained also for any individually used model (Figures S2–S4 in Supporting Information S1). We further note that although the number of

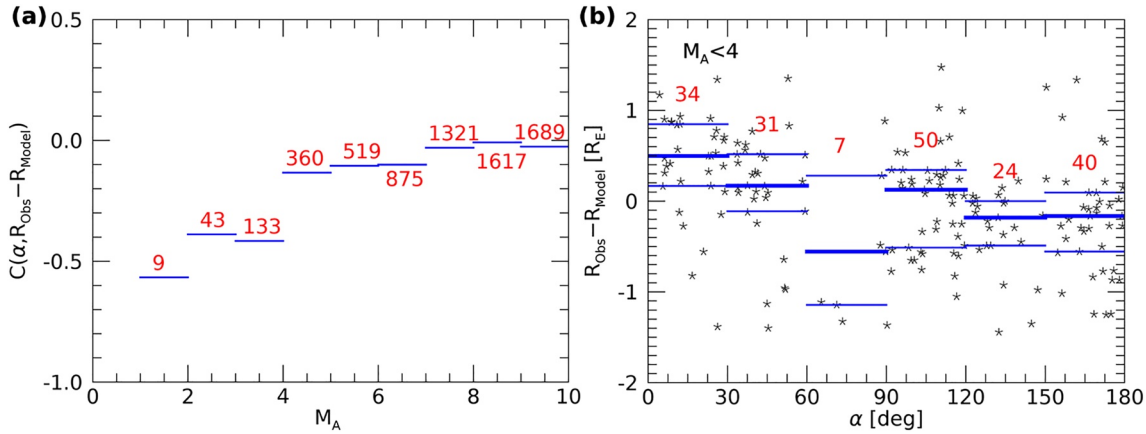

Figure 4. (a) Correlation between α, that is, the angle between the projections of the crossing positional vector and the interplanetary magnetic field vector to the y-z plane, and the difference between observed and model magnetopause distance as a function of the Alfvén Mach number. The number of crossings in each interval is mentioned. (b) Difference between observed and model magnetopause distance as a function of α. The horizontal blue lines show the medians and 0.25 and 0.75 quartiles in the respective intervals. Only the magnetopause crossings obtained during low Alfvén Mach numbers ($M_A < 4$) are considered. The number of crossings in each interval is mentioned.

magnetopause crossings under the extreme IMF B_y values is very limited, the distribution of their z_{GSM} coordinate remains roughly symmetric around the ecliptic plane both for IMF $B_y > 8$ and IMF $B_y < -8$ nT.

The locations of crossings are divided into two regions, $y_{GSM} > 2\ R_E$ and $y_{GSM} < -2\ R_E$, corresponding to the afternoon and morning sectors in Figure 3. It turns out that $R_{Obs} - R_{Model}$ in these regions is controlled by the sign of the IMF B_y. Figure 3a shows the histogram of $R_{Obs} - R_{Model}$ obtained for IMF $B_y > 8$ nT at $y_{GSM} > 2\ R_E$. The median value of the differences, marked by the thick vertical red line, is about $+0.22\ R_E$. The thinner red vertical lines correspond to 0.25 and 0.75 quartiles of the distribution. Figure 3b shows the histogram of the $R_{Obs} - R_{Model}$ obtained for IMF $B_y > 8$ nT, but this time at locations $y_{GSM} < -2\ R_E$. The median value of the differences in this case is about $-0.20\ R_E$. Although the number of relevant magnetopause crossings is very limited, these results indicate that the magnetopause distances are larger in the y_{GSM} sector corresponding to the orientation of IMF B_y. This is further confirmed by the results depicted in Figures 3c and 3d, which use the same representation to study the distribution of $R_{Obs} - R_{Model}$ for IMF $B_y < -8$ nT. This time the situation is reversed and the median differences are lower in the $y_{GSM} > 2\ R_E$ sector (Figure 3c, about $-0.10\ R_E$) and larger in the $y_{GSM} < -2\ R_E$ sector (Figure 3d, about $0.71\ R_E$). This essentially means that the magnetopause appears to move in the direction of B_y rather than being simply symmetrically elongated along/opposite the B_y direction.

We further define the angle α between the projections of the positional vector of a given magnetopause crossing and the IMF vector to the y-z plane. Since Lavraud et al. (2013) suggested magnetopause elongation for low Mach number solar wind, Figure 4a investigates the range of Alfvén Mach numbers for which the effect is eventually present. For this purpose, we divide the magnetopause crossings into intervals according to the Alfvén Mach number. The number of magnetopause crossings in individual Alfvén Mach number intervals is shown by the red numbers. In each interval, the Spearman's rank correlation coefficient between the angle α and $R_{Obs} - R_{Model}$ is evaluated. It can be seen that the largest negative correlation is observed for the lowest Alfvén Mach numbers. For larger Alfvén Mach numbers, the correlation coefficient gradually approaches zero and the correlation eventually nearly disappears for $M_A > 4$.

The situation under low Alfvén Mach numbers is depicted in Figure 4b. Each point corresponds to a single magnetopause crossing under $M_A < 4$. The horizontal lines mark the first quartile, median, and the third quartile in the 30° wide α bins. The results indeed show that $R_{Obs} - R_{Model}$ is larger for values of α close to 0° (positional vector of the crossing and IMF in the same direction), while they are lower for values of α close to 180° (positional vector of the crossing and IMF in opposite directions). This means that changing the IMF direction to the opposite would change the magnetopause location, that is, the orientation of the IMF vector apparently plays the role. Although the scatter is large and the number of data points is quite limited (186 crossings), a systematic decreasing trend for the $R_{Obs} - R_{Model}$ with α can be seen. The corresponding Spearman's rank correlation coefficient is about −0.39 and the relation is statistically significant with a 99.9% confidence. We note

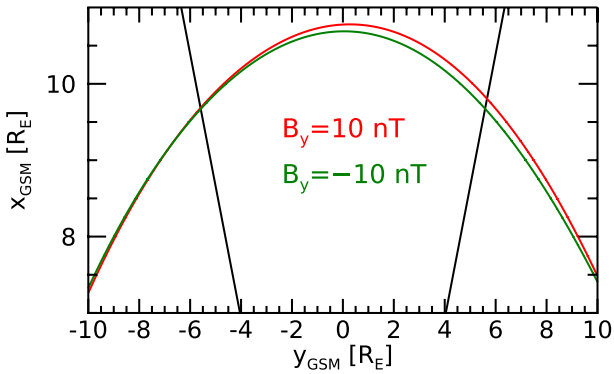

Figure 5. Model magnetopause shapes obtained for large positive and large negative interplanetary magnetic field B_y component are shown by the red and green curves, respectively. The black lines correspond to the region within ±30° from the subsolar point.

that although the average model prediction based on the three considered empirical magnetopause models is again used, essentially the same result is obtained also when any of the models is used individually (Figure S5 in Supporting Information S1).

4. Discussion

A data set of the nearly 50,000 magnetopause crossings identified in the THEMIS A-E, Magion 4, Geotail, and Interball satellite data is used as a starting point of the present study. The limitation to within 30° from the subsolar point leaves us with as many as 14,781 magnetopause crossings for the analysis. These crossings are limited to the vicinity of the ecliptic plane, and virtually unaffected by the cusp indentations and sampling bias due to the limited spacecraft apogee. In order to investigate possible IMF clock angle effects on the magnetopause location, we need to account for much stronger effects due to the solar wind dynamic pressure and IMF B_z component. This is achieved by analyzing the values of $R_{Obs} - R_{Model}$ rather than the observed distances themselves. Three different empirical models are used for this purpose (Lin et al., 2010; Petrinec & Russell, 1996; Shue et al., 1997), all parameterized by the solar wind dynamic pressure and IMF B_z and providing essentially the same results. The arithmetic mean of the three empirical model predictions is thus eventually used in the analysis.

The performed analysis demonstrates that the IMF clock angle and, in particular, IMF B_y is possibly an important factor affecting the magnetopause distance, but it is not included in the models. The magnetopause distances are larger than predicted at the times of low IMF B_y. This seems to contradict the results obtained by Case and Wild (2013), who found little to no influence of the clock angle on the magnetopause radial distance. However, the discrepancy may be possibly attributed to our data set limited to the vicinity of the subsolar point and thus arguably better suited for the identification of subtle changes of the magnetopause distance. We note that, according to Dušík et al. (2010) and Samsonov et al. (2012), the magnetopause distances are typically larger at the times of the radial IMF, which corresponds to a subset of crossings with low IMF B_y.

Although the number of crossings at the times of large IMF B_y is considerably limited, the respective results indicate that not only the IMF B_y magnitude, but also the IMF B_y direction is important, eventually introducing a considerable dawn-dusk asymmetry of magnetopause. Specifically, the magnetopause crossing distances appear to be larger in the y sector where the IMF B_y points. This is further confirmed by analysis of the dependence of $R_{Obs} - R_{Model}$ on the angle between the IMF vector and the magnetopause crossing vector (in the y-z plane). It shows that the magnetopause crossings tend to be observed at larger distances at the times of the IMF vector pointing in the direction of the magnetopause crossing, while they tend to be observed at lower distances when the IMF vector points in the opposite direction. The effect is observed only for a very low Alfvén Mach number ($M_A < 4$) and eventually disappears as the Alfvén Mach number increases. This dependence appears to be rather consistent with the effect reported by Lavraud et al. (2013) and Liu et al. (2015). However, their results suggested an elongation of the magnetopause shape along IMF, that is, larger radial distances both in the IMF vector direction and opposite to the IMF vector direction. On the other hand, our results indicate an asymmetric situation, corresponding rather to the magnetopause shift than to the magnetopause elongation.

It is instructive to check whether our experimental result is consistent with global MHD simulation results. For this purpose, we use MHD runs publicly available at CCMC. The runs Gabrielle_Lefebvre_032718_9b and Gabrielle_Lefebvre_032718_10b well fit the conditions where the effect might be anticipated and have a fine resolution on the dayside (1/8 R_E). They use the Space Weather Modeling Framework v20140611 model coupled with the ring current model and auroral ionospheric conductance. The runs use the solar wind velocity of 400 km/s, solar wind density of 5 cm^{-3}, and two possible values of IMF B_y, either $B_y = 10$ nT or $B_y = -10$ nT (while $B_x = 0$ nT and $B_z = 0$ nT). This corresponds to the Alfvén Mach number of about 4.1. The model output provides, among other parameters, the current density in the y direction (j_y), whose local maximum corresponding to the Chapman-Ferraro current is used to identify the magnetopause location (Němeček et al., 2011). The resulting magnetopause locations for the two runs are shown in Figure 5 by the red and green curves, respectively. Considering that, apart from the B_y direction, all other parameters are the same, it is interesting to note that the

model magnetopause locations are indeed different. Moreover, the observed differences roughly correspond to the aforementioned experimental results. At $y_{GSM} > 0$, the model magnetopause is located at larger distances during positive IMF B_y than during negative IMF B_y. At $y_{GSM} < 0$, the difference between respective magnetopause distances is very small, but there is a hint of the distances being larger for negative IMF B_y. The difference of the magnetopause distances for the two model runs gets as large as about 0.2 R_E. These modeling results seem to be at least qualitatively consistent with the observations. We do not have any clear explanation at the moment. We believe that, in line with former studies, the asymmetry may possibly arise in the magnetosheath (Longmore et al., 2005). Alternatively, one should perhaps consider also possible asymmetries formed in the magnetosphere (Dmitriev et al., 2004). We note that the model magnetospheric j_y current distribution is indeed different for the positive IMF B_y and negative IMF B_y (see Figure S6 in Supporting Information S1).

5. Conclusions

We used a data set of as many as 14,781 magnetopause crossings within 30° from the subsolar point compiled from several different spacecraft data to investigate a possible IMF effect on the magnetopause location. In order to eliminate the strong controlling role of the solar wind dynamic pressure and IMF B_z component, $R_{Obs} - R_{Model}$ values were analyzed rather than the magnetopause distances themselves. Three different empirical magnetopause models were used for this purpose, all providing qualitatively the same results.

We have shown that the IMF clock angle is an important factor controlling the magnetopause location. In particular, the magnetopause is found at larger radial distances at the times of low IMF B_y component. Furthermore, not only the IMF B_y magnitude but also the IMF B_y orientation was found to be of importance, resulting in possible magnetopause asymmetry. Although the number of crossings under the given extreme conditions considered (IMF $B_y > 8$ or IMF $B_y < -8$ nT) is rather limited (121 and 136 crossings, respectively), a systematic expansion of the magnetopause location is observed in the dawn/dusk region depending on the orientation of IMF B_y.

This effect is further confirmed by considering the angle between the IMF vector and the magnetopause crossing vector (both projected to the y-z plane). For low Alfvén Mach numbers ($M_A < 4$), the magnetopause distances tend to be larger when the IMF vector points along the respective magnetopause crossing vector, while the magnetopause distances tend to be lower when the IMF vector points opposite to the magnetopause crossing vector. These experimental results are qualitatively consistent with publicly available global MHD simulation runs.

Data Availability Statement

The used magnetic field and plasma data can be accessed from open-access sources via http://cdaweb.gsfc.nasa.gov/cdaweb. The Community Coordinated Modeling Center model runs Gabrielle_Lefebvre_032718_9b and Gabrielle_Lefebvre_032718_10b can be accessed from https://ccmc.gsfc.nasa.gov/results/viewrun.php?domain=GM&runnumber=Gabrielle_Lefebvre_032718_9b and https://ccmc.gsfc.nasa.gov/results/viewrun.php?domain=GM&runnumber=Gabrielle_Lefebvre_032718_10b, respectively.

Acknowledgments
The authors thank all the spacecraft teams for the magnetic field and plasma data and the Community Coordinated Modeling Center for modeling support. The work was supported by the Czech Science Foundation under Contract 21-26463S.

References

Boardsen, S., Eastman, T., Sotirelis, T., & Green, J. (2000). An empirical model of the high-latitude magnetopause. *Journa l of Geophysical Research*, *105*(A10), 23193–23219. https://doi.org/10.1029/1998JA000143

Cahill, L., & Amazeen, P. (1963). The boundary of the geomagnetic field. *Journal of Geophysical Research*, *68*(7), 1835–1843. https://doi.org/10.1029/JZ068i007p01835

Case, N., & Wild, J. (2013). The location of the Earth's magnetopause: A comparison of modeled position and in situ cluster data. *Journal of Geophysical Research: Space Physics*, *118*(10), 6127–6135. https://doi.org/10.1002/jgra.50572

Dmitriev, A. V., Suvorova, A. V., Chao, J. K., & Yang, Y. (2004). Dawn-dusk asymmetry of geosynchronous magnetopause crossings. *Journal of Geophysical Research*, *109*(A5), A05203. https://doi.org/10.1029/2003JA010171

Dušík, Š., Granko, G., Šafránková, J., Němeček, Z., & Jelínek, K. (2010). IMF cone angle control of the magnetopause location: Statistical study. *Geophysical Research Letters*, *37*(19), L19103. https://doi.org/10.1029/2010GL044965

Fairfield, D. H. (1971). Average and unusual locations of the Earth's magnetopause and bow shock. *Journal of Geophysical Research*, *76*(28), 6700–6716. https://doi.org/10.1029/JA076i028p06700

Formisano, V., Domingo, V., & Wenzel, K. (1979). The three-dimensional shape of the magnetopause. *Planetary and Space Science*, *27*(9), 1137–1149. https://doi.org/10.1016/0032-0633(79)90134-X

Grygorov, K., Němeček, Z., Šafránková, J., Šimůnek, J., & Gutynska, O. (2022). Storm-time magnetopause: Pressure balance. *Journal of Geophysical Research: Space Physics*, *127*(11), e2022JA030803. https://doi.org/10.1029/2022JA030803

Haaland, S., Hasegawa, H., Paschmann, G., Sonnerup, B., & Dunlop, M. (2021). 20 years of Cluster observations: The magnetopause. *Journal of Geophysical Research: Space Physics*, *126*(8), e2021JA029362. https://doi.org/10.1029/2021JA029362

Lavraud, B., & Borovsky, J. (2008). Altered solar wind-magnetosphere interaction at low Mach numbers: Coronal mass ejections. *Journal of Geophysical Research*, *113*(A9), A00B08. https://doi.org/10.1029/2008JA013192

Lavraud, B., Larroque, E., Budnik, E., Génot, V., Borovsky, J., Dunlop, M., et al. (2013). Asymmetry of magnetosheath flows and magnetopause shape during low Alfvén Mach number solar wind. *Journal of Geophysical Research: Space Physics*, *118*(3), 1089–1100. https://doi.org/10.1002/jgra.50145

Lin, R., Zhang, X., Liu, S., Wang, Y., & Gong, J. (2010). A three-dimensional asymmetric magnetopause model. *Journal of Geophysical Research*, *115*(A4), A04207. https://doi.org/10.1029/2009JA014235

Liu, Z., Lu, J., Wang, C., Kabin, K., Zhao, J., Wang, M., et al. (2015). A three-dimensional high Mach number asymmetric magnetopause model from global MHD simulation. *Journal of Geophysical Research: Space Physics*, *120*(7), 5645–5666. https://doi.org/10.1002/2014JA020961

Longmore, M., Schwartz, S. J., Geach, J., Cooling, B. M. A., Dandouras, I., Lucek, E. A., & Fazakerley, A. N. (2005). Dawn-dusk asymmetries and sub-Alfvénic flow in the high and low latitude magnetosheath. *Annales Geophysicae*, *23*(10), 3351–3364. https://doi.org/10.5194/angeo-23-3351-2005

Lu, J., Liu, Z.-Q., Kabin, K., Jing, H., Zhao, M., & Wang, Y. (2013). The IMF dependence of the magnetopause from global MHD simulations. *Journal of Geophysical Research: Space Physics*, *118*(6), 3113–3125. https://doi.org/10.1002/jgra.50324

Machková, A., Němec, F., Němeček, Z., & Šafránková, J. (2019). On the influence of the Earth's magnetic dipole eccentricity and magnetospheric ring current on the magnetopause location. *Journal of Geophysical Research: Space Physics*, *124*(2), 905–914. https://doi.org/10.1029/2018JA026070

Němeček, Z., Šafránková, J., Koval, A., Merka, J., & Přech, L. (2011). MHD analysis of propagation of an interplanetary shock across magnetospheric boundaries. *Journal of Atmospheric and Solar-Terrestrial Physics*, *73*(1), 20–29. https://doi.org/10.1016/j.jastp.2010.05.017

Němeček, Z., Šafránková, J., Lopez, R. E., Dušík, Š., Nouzák, L., Přech, L., et al. (2016). Solar cycle variations of magnetopause locations. *Advances in Space Research*, *58*(2), 240–248. https://doi.org/10.1016/j.asr.2015.10.012

Němeček, Z., Šafránková, J., & Šimůnek, J. (2020). An examination of the magnetopause position and shape based upon new observations. In *Dayside magnetosphere interactions* (pp. 135–151). American Geophysical Union (AGU). https://doi.org/10.1002/9781119509592.ch8

Nguyen, G., Aunai, N., Michotte de Welle, B., Jeandet, A., Lavraud, B., & Fontaine, D. (2021a). Massive multi-mission statistical study and analytical modeling of the Earth's magnetopause: 2. Shape and location. *Journal of Geophysical Research: Space Physics*, *127*(1), e2021JA029774. https://doi.org/10.1029/2021JA029774

Nguyen, G., Aunai, N., Michotte de Welle, B., Jeandet, A., Lavraud, B., & Fontaine, D. (2021b). Massive multi-mission statistical study and analytical modeling of the Earth's magnetopause: 3. An asymmetric non indented magnetopause analytical model. *Journal of Geophysical Research: Space Physics*, *127*(1), e2021JA030112. https://doi.org/10.1029/2021JA030112

Petrinec, S., & Russell, C. (1996). Near-Earth magnetotail shape and size as determined from the magnetopause flaring angle. *Journal of Geophysical Research*, *101*(A1), 137–152. https://doi.org/10.1029/95JA02834

Šafránková, J., Dušík, Š., & Němeček, Z. (2005). The shape and location of the high-latitude magnetopause. *Advances in Space Research*, *36*(10), 1934–1939. https://doi.org/10.1016/j.asr.2004.05.009

Šafránková, J., Němeček, Z., Dušík, Š., Přech, L., Sibeck, D. G., & Borodkova, N. N. (2002). The magnetopause shape and location: A comparison of the Interball and Geotail observations with models. *Annales Geophysicae*, *20*(3), 301–309. https://doi.org/10.5194/angeo-20-301-2002

Samsonov, A., Němeček, Z., Šafránková, J., & Jelínek, K. (2012). Why does the subsolar magnetopause move sunward for radial interplanetary magnetic field? *Journal of Geophysical Research*, *117*(A5), A05221. https://doi.org/10.1029/2011JA017429

Shue, J., Chao, J., Fu, H., Russell, C., Song, P., Khurana, K., & Singer, H. (1997). A new functional form to study the solar wind control of the magnetopause size and shape. *Journal of Geophysical Research*, *102*(A5), 9497–9511. https://doi.org/10.1029/97JA00196

Spreiter, J., Summers, A., & Alksne, A. Y. (1966). Hydromagnetic flow around the magnetosphere. *Planetary and Space Science*, *14*(3), 223–253. https://doi.org/10.1016/0032-0633(66)90124-3

Turc, L., Tarvus, V., Dimmock, A. P., Battarbee, M., Ganse, U., Johlander, A., et al. (2020). Asymmetries in the Earth's dayside magnetosheath: Results from global hybrid-Vlasov simulations. *Annales Geophysicae*, *38*(5), 1045–1062. https://doi.org/10.5194/angeo-38-1045-2020